A new approach for quantitative mapping of retention mechanisms of associative polymers in porous media.

AFOLABI, R.O., OLUYEMI, G.F., OFFICER, S. and UGWU, J.O.

2021

Research Article

Title: A New Approach for Quantitative Mapping of Retention Mechanisms of Associative Polymers in Porous Media.

Authors: Richard O. Afolabi[1, *], Gbenga F. Oluyemi[1], Simon Officer[2], Johnson O. Ugwu[3].

Affiliations: [1] Petroleum Engineering Research Group (PERG), School of Engineering, Robert Gordon University, Aberdeen, AB10 7GJ, United Kingdom.

[2] School of Pharmacy and Life Sciences, Robert Gordon University, Aberdeen, AB10 7GJ, United Kingdom.

[3] School of Science, Engineering and Design, Teesside University, Middlesbrough, Tees Valley, TS1 3BX, United Kingdom.

***Contact email**: r.afolabi@rgu.ac.uk

Abstract

The retention of associative polymer molecules poses a significant challenge for its transport in porous media, and this arises due to the hydrophobic interactions that exists between the retained molecules. The known experimental approach in literature for quantifying polymer retention under static or dynamic conditions reports a generalized outcome without adequate estimates for each type of retention mechanisms. Thus, an accurate quantitative description of the various retention mechanisms (monolayer adsorption, multilayer adsorption and entrapment) attributable to associative polymers is crucial for proper optimization of its transport in porous media. In this work, a novel predictive approach was developed for quantitative mapping of the various retention mechanisms connected with associative polymers. The basis was a first-principles method adopted in mapping static to dynamic retention. This novel approach was achieved by relating the characteristic time scale for static and dynamic retention to the variation in polymer and reservoir properties, thus making it possible to correlate static retention results to large-scale dynamic retention with minimal fitting parameters. Furthermore, the mapping of the static to dynamic retention ensured an accurate quantification of the different retention mechanisms attributable to associative polymers. In this model, the in-situ entrapment was linked to the effective pore radius and the hydrodynamic size of the polymer molecules. Entrapment of polymer molecular aggregates was predicted based on the assumption that this occurs when the hydrodynamic size of the molecules becomes equal/greater than the effective pore size in the porous media. In addition, a threshold concentration value was estimated from which mechanical entrapment of polymer molecules would occur in a porous media alongside adsorption on pore surface. Similarly, a concentration value was estimated at which entrapment of polymer molecules becomes the dominant retention mechanism in the porous media.

Keywords: Associative Polymers; Adsorption; Polymer Retention; Mechanical Entrapment.

1. Introduction

The retention mechanism of polymer molecules when transported in a porous media occur in in the form of adsorption and entrapment (Al-Hajri et al., 2018; Al-Hajri et al., 2019; Al-Hajri et al., 2020). However, these mechanisms are slightly different for associative polymers and makes their interaction with the pore surface distinctive from non-associative polymers (Afolabi, 2015; El-Hoshoudy et al., 2017; Bai et al., 2018). In the case of adsorption, associative polymers have been reported to take place as monolayer and multilayer adsorption phenomenon whereas for non-associative polymers this occurs as monolayer adsorption (Seright et al., 2011; Guo et al., 2016; Afolabi et al., 2019a; Afolabi et al., 2019b). The concept of multilayer adsorption arises due to hydrophobic interactions between the adsorbed polymer molecules and bulk molecules at the centre of the flow channels. The other form of retention of associative polymer molecules in a porous media is the entrapment of molecular aggregates (Li et al., 2016; Quan et al., 2019). Entrapment of associative polymers arises when molecules interact due to hydrophobic association to form aggregates with molecular size greater than the original hydrodynamic size of a single polymer molecule. Apparently, aggregation of polymer molecules occurs in the semi-dilute concentration regime where polymer concentration exceeds the critical aggregation concentration (C_{ag}) (Li-Bin et al., 2010; Guo et al., 2012; Kamal et al., 2015; Quan et al., 2016; Jincheng et al., 2018). Therefore, operating at a polymer concentration above the C_{ag} of the polymer could lead to entrapment of polymer molecular aggregates in a porous media. A significant challenge with the entrapment of polymer aggregates is that it negates the propagation of the desired viscous properties of associative polymers deep into the porous media (Zhang et al., 2014; Yekeen et al., 2017; Torrealba et al., 2019). The well-established experimental methodologies for quantifying polymer retention in porous media have been reported as the dynamic and the static retention test (Al-Hajri et al., 2019; Al-Hajri et al., 2020). However, these techniques do not uniquely map and quantify the

71 various retention mechanisms. Rather, a generalized output is obtained from these experimental
72 techniques with no clear distinction between the contributions of the various mechanisms
73 associated with polymer retention. For example, the dynamic retention test gives a more
74 detailed account of polymer retention in a porous media, but the experimental accuracy in
75 indicating the various retention mechanisms is limited (Zhang et al., 2014; Yekeen et al., 2017;
76 Torrealba et al., 2019; Afolabi et al., 2020). Effluent concentration profiles from polymer
77 injection in a porous media can indicate incremental retention with changing flow conditions.
78 Zhang (2013) reported that hydrodynamic entrapment of polymer molecules arising from
79 changing flow rate could be studied by monitoring the concentration of effluent solutions. A
80 decrease in the effluent concentration with increased flow rate indicates hydrodynamic
81 entrapment. An increase in effluent concentration with a reduced flow rate implies releasing
82 the entrapped molecules back to the mainstream. This was further corroborated by the works
83 of Zhang et al. (2014) and Idahosa et al. (2016) on rate-dependent polymer retention in porous
84 media. Idahosa et al. (2016) showed that incremental retention due to rate increase or decrease
85 could be monitored by evaluating the concentration of the effluent solution from the porous
86 media. This approach was modelled according to Zhang (2013) and Zhang et al. (2014).
87 However, the known and established experimental procedure for the dynamic retention test in
88 porous media cannot account for the distribution of these retained polymer molecules around
89 the various mechanisms. In other words, the outcome of this widely adopted procedure for
90 dynamic retention test cannot indicate:

91 a) The proportion of the total polymer retention that can be assigned to mechanical entrapment
92 and adsorption.

93 b) If the additional retained molecules arising from incremental flow rate would either
94 contribute to the existing adsorption or entrapment or both at the same time.

In like manner, a predictive approach for the quantification of the various retention mechanisms in a porous media reported in literature is not well understood. Nevertheless, the predictive approach is considered important for the purpose of computational modelling, economic planning and polymer performance forecasting. Therefore, accurate prediction and quantification of entrapped aggregates is significant as operating with polymer concentration with substantial number of aggregates each time the size greater than the pore size could indicate considerable loss of molecules to entrapment with negative economic impact. Consequently, this work proposes an innovative and novel approach towards mapping static to dynamic adsorption and quantifying the various mechanisms associated with polymer retention in a porous media. The proposed approach was developed in such a way to be generic irrespective of the type of polymer: associative or non-associative. In addition, this novel approach ensures the prediction of the onset of hydrodynamic entrapment of polymer molecular aggregates in a porous media. In addition, this approach of predicting the onset of hydrodynamic entrapment takes into account a threshold concentration value based on the knowledge of the average pore radius of the porous media and the average hydrodynamic radius of the polymer molecules from which entrapment becomes the dominant mechanism for polymer retention.

2. Predictive Approach for Quantification of Polymer Retention Mechanisms

2.1. Mapping Static to Dynamic Retention

A constant denominator for static and dynamic retention is the "**Contact Time**" for surface interaction (Kajjumba et al., 2018). This is further shown in Table 1 when comparing the various adsorption kinetic models. Thus, the following general expression between the amount of polymer retained at a given time, Γ_p and the contact time for the static retention process, t_c is given in equation (1)

Table 1: *Some of the known kinetic models used in the study of polymer adsorption (Kajjumba et al., 2018).*

Name	Equation	Parameters	Remarks
Pseudo First Order Model	$\frac{d\Gamma_t}{dt} = k(\Gamma_e - \Gamma_t)$	Γ_t is the adsorbate on adsorbent in time, t, Γ_e is the equilibrium adsorption capacity and k is the rate constant.	The common denominator in each model is the independent time factor
Pseudo Second Order Model	$\frac{d\Gamma_t}{dt} = k(\Gamma_e - \Gamma_t)^2$	Γ_t is the adsorbate on adsorbent in time, t, Γ_e is the equilibrium adsorption capacity and k is the rate constant.	
Elovich Model	$\frac{d\Gamma_t}{dt} = \alpha\left(\exp^{-\beta\Gamma_t}\right)$	Γ_t is the adsorbate on adsorbent in time, t, α is the initial adsorption rate and β is the desorption constant.	
Webb and Morris Model	$\Gamma_t = K_p\sqrt{t} + C$	K_p is the rate constant and C is the boundary layer thickness which determines the boundary layer effect.	
Boyd Model	$\frac{\Gamma_t}{\Gamma_\infty} = 1 - \frac{6}{\pi^2}\sum_{1}^{\infty}\left(\frac{1}{n^2}\right)\exp\left(-n^2 B_t\right)$	Γ_∞ is the adsorbate at infinite time, B_t is a mathematical function of the ratio $\frac{\Gamma_t}{\Gamma_\infty}$	

$$\Gamma_p \propto t_c \quad (1)$$

Equation (1) can be simplified into (2) by introducing a constant, K_c as shown below:

$$\Gamma_p = K_c t_c \quad (2)$$

According to Lohne et al. (2017), the rotational diffussion, D_{rot} of the polymer molecules can be related to a characteristic time scale, t_c as shown in (3)

$$t_c = \frac{1}{2D_{rot}} \quad (3)$$

This diffussion coefficient was computed using the Einstein–Smoluchowski relation in (4)

$$D_{rot} = \frac{k_B T}{8\pi\mu_s R_h^3} \quad (4)$$

Where k_B is the Boltzmann constant and R_h is the hydrodynamic radius of a rigid sphere of a flexible polymer in solution. Substituting (4) into (3),

$$t_c = \frac{4\pi\mu_s R_h^3}{k_B T} \quad (5)$$

The value of R_h is estimated using the expression given by Lohne et al. (2017) in equation (6)

$$R_h = \left(\frac{3}{10\pi N_A}\right)^{1/3} ([\mu]M_w)^{1/3} \quad (6)$$

Where N_A is the Avogadro's number. Combining (5) and (6), a new expression for t_c is in (7)

$$t_c = \left(\frac{6}{5k_B N_A}\right)\left(\frac{\mu_s[\mu]M_w}{T}\right) \quad (7)$$

Therefore, a modified relationship between the static retention, Γ_{p-st} and the contact time, t_c becomes equation (8):

$$\Gamma_{p-st} = K_c\left[\left(\frac{6}{5k_B N_A}\right)\left(\frac{\mu_s[\mu]M_w}{T}\right)\right] \quad (8)$$

According to Lohne et al. (2017), computation of the pore residence time for dynamic retention can be made based on the assumption that the pore length, L_p is equal to the grain size, D_g. This holds true for simple granular porous media composed of clean sands and sandstones (Bernabe et al., 2011; Revil et al., 2012). As such, the pore radius, R_p is given in (9)

$$\frac{2\phi}{R_p} = 6\frac{(1-\phi)}{D_g} = 6\frac{(1-\phi)}{L_p} \quad (9)$$

The grain size, D_g or L_p can be calculated as the representative grain size for a packed bed of mono-sized spherical particles using the Blake-Kozeny equation (Brakstad and Rosenkilde, 2016). Therefore, the pore residence time can be computed as shown in (10)

$$\tau_r = \frac{L_p}{v_p} = 12\left(\frac{1-\phi}{\phi\gamma}\right) \quad (10)$$

Where v_p is the average pore velocity and $\gamma = 4v_p/R_p$ relates the shear rate at the wall to the average pore velocity. Therefore, the contact time under dynamic conditions becomes (11):

$$\tau_c = 12\left(\frac{1-\phi}{\phi\gamma}\right) \quad (11)$$

Thus, a modified relationship between the dynamic retention, Γ_{p-dy} and the contact time, t_c becomes equation (12):

$$\Gamma_{p-dy} = K_c\left[12\left(\frac{1-\phi}{\phi\gamma}\right)\right] \quad (12)$$

The correlation between static and dynamic retention was obtained as shown in (13):

$$\frac{\Gamma_{p-dy}}{\Gamma_{p-st}} = \frac{K_c\left[12\left(\frac{1-\phi}{\phi\gamma}\right)\right]}{K_c\left[\left(\frac{6}{5k_BN_A}\right)\left(\frac{\mu_s[\mu]M_w}{T}\right)\right]} \quad (13)$$

The ratio of the contact times on the right-hand side (RHS) of equation (13) is related to the Deborah number, N_{De} which is defined as the ratio of the polymer relaxation time to the pore residence time.

$$N_{De} = \frac{\left[\left(\frac{6}{5k_BN_A}\right)\left(\frac{\mu_s[\mu]M_w}{T}\right)\right]}{\left[12\left(\frac{1-\phi}{\phi\gamma}\right)\right]} \quad (14)$$

Therefore, equation (13) becomes (15)

$$\Gamma_{p-dy} = \left(\frac{1}{N_{De}}\right)\Gamma_{p-st} \quad (15)$$

Thus, static retention can be mapped into dynamic retention using equation (15).

2.2. Quantification of Polymer Retention Mechanisms in Porous Media

2.2.1. Hydrophobic Interactions Between Retained Polymer Molecules

In defining a parameter that quantifies the proportion of hydrophobic interactions between associative polymer chains retained on a pore surface, the following assumptions were made:

a) The hydrophobic interaction network between polymer chains only takes place in the semi-dilute concentration regime, i.e., polymer concentration, C_p must be greater than the critical aggregation concentration, C_{ag}.

b) The increase in polymer concentration, C_p (beyond C_{ag}) would lead to a rise in the proportion of hydrophobic interactions and a reduction in the proportion of intramolecular interactions.

Based on the assumptions highlighted above, the following dimensionless parameter, H_i was used to quantify the hydrophobic interactions between associative polymer chains in (16):

$$H_i = \frac{C_p - C_{ag}}{C_p} \begin{cases} C_p > C_{ag} \\ C_{ag} \neq 0 \end{cases} \tag{16}$$

2.2.2. Fractional Damaged Pore Volume and Interactions within Retained Polymers

For accurate mapping of static to dynamic interactions, the fractional damaged pore volume (DPV or Γ_D) is related to (13) as shown in (17):

$$\Gamma_D = \frac{\Gamma_{p-dy}}{\Gamma_{p-st}} = \frac{\left[12\left(\frac{1-\phi}{\phi\gamma}\right)\right]}{\left[\left(\frac{6}{5k_B N_A}\right)\left(\frac{\mu_s[\mu]M_W}{T}\right)\right]} \tag{17}$$

Modifying equation (17) based on the first order approximation of the Huggins equation and incorporation of (16) results in (18):

$$1 - H_i = \frac{5R_g T(1-\phi)\Gamma_D C_{ag}}{3\mu_s \mu_{sp} \phi \gamma M_W} \tag{18}$$

Equation (18) predicts the proportion of hydrophobic interactions between retained molecules.

2.2.3. Predicting Retention Mechanisms in Porous Media

Table 2 gives the various conditions for mapping the known mechanisms associated with polymer retention. The cumulative size distribution of the retained polymer molecules was estimated based on the assumption that the cumulative amount of retained polymer molecules increases with injection concentration as shown in (19)

$$\mathrm{Ret}_{(C_{pi})} \cong \mathrm{Ret}_{\sum_{i=1}^{n} C_{p_{i-1}}} \quad (19)$$

Where $\mathrm{Ret}_{(C_{pi})}$ is the retained polymer at concentration C_{pi} and $\mathrm{Ret}_{\sum_{i=1}^{n} C_{p_{i-1}}}$ is the cumulative retained polymer from concentrations C_{po} up to C_{pi}.

Table 2*: Conditions for distinguishing between the different retention mechanism in a porous media. R_h is the hydrodynamic size of the polymer; R_{hi} is the size of the retained polymer molecule and R_p is the pore size of the porous media (Al-Hajri et al., 2018; Al-Hajri et al., 2020).*

Conditions	Meaning
$R_{hi} < R_p$	Adsorption
$R_h < R_{hi} < R_p$	Multilayer Adsorption
$R_{hi} \approx R_p$	Entrapment
$R_{hi} > R_p$	Pore Plugging

The size distribution of the retained polymer molecules, R_{hi} was estimated using a modified form of the expression by Lohne et al. (2017) as shown in (20)

$$R_{hi} = R_h \left[\frac{C_p}{C_{ag}}\right]^{H_i} \quad (20)$$

Where R_h is the hydrodynamic radius of the molecules which is given in equation (21) and H_i is proportion of hydrophobic interactions among the retained molecules in (18).

$$R_h = \left(\frac{3}{10\pi N_A}\right)^{1/3} ([\mu]M_w)^{1/3} \quad (21)$$

Figure 1 shows the plot of the cumulative pore size distribution, $f(R_p)$ and the cumulative size distribution of the retained polymer molecules, $f(R_h)$. The pore fraction of entrapped molecules, Γ_{ent} up to R_2 can be predicted using equation (22)

$$\Gamma_{ent} = \int_{R_{p1}}^{R_{p2}} f(R_p) / \int_{R_o}^{R_{h2}} f(R_h) \quad (22)$$

The inaccessible pore volume, I_{PV} is computed using equation (23)

$$I_{PV} = \int_{R_{p1}}^{R_{p2}} f(R_p) / \int_{R_{p1}}^{R_{p3}} f(R_p) \quad (23)$$

However, the I_{PV} in this work is defined as the sum of the pore fraction completely accessible to brine, I_{PVo} and that lost to entrapped molecules, Γ_{ent} as shown in (24)

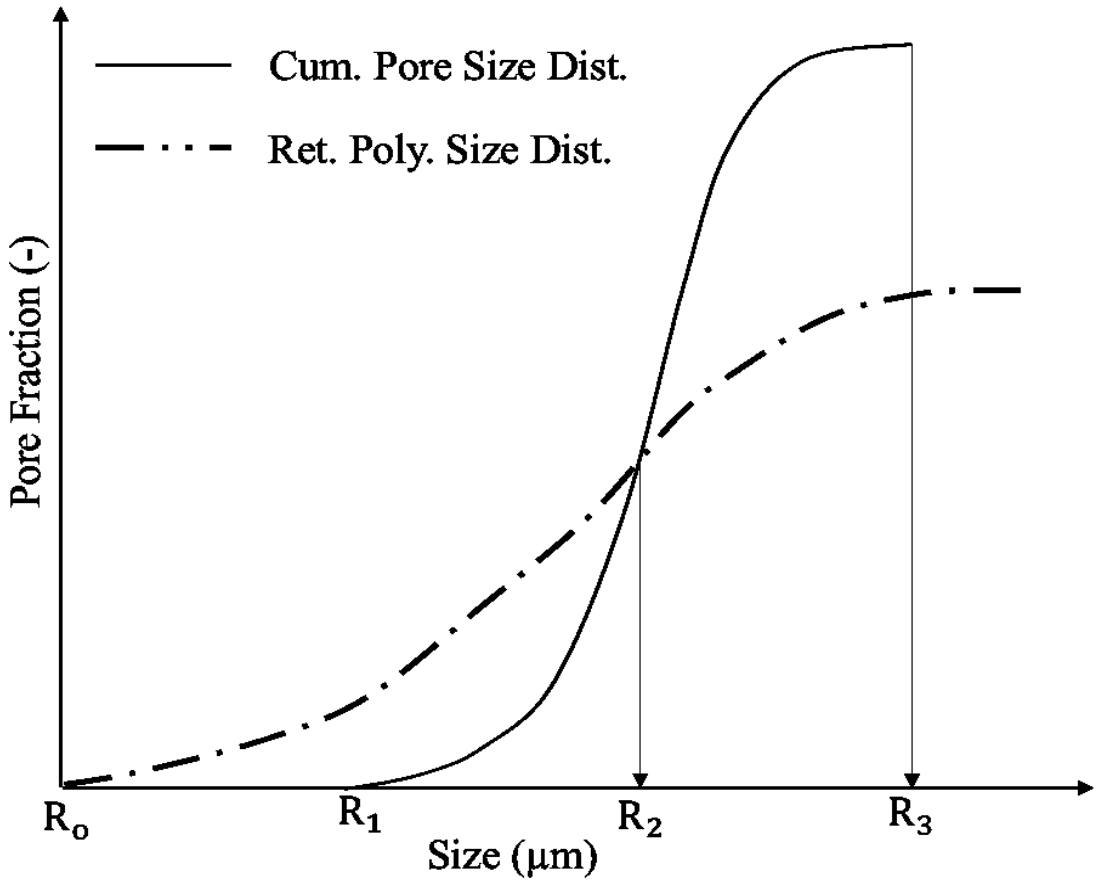

***Figure 1**: Plot of pore size distribution and the cumulative size distribution of the retained polymer molecules in the porous media. The point* R_2 *was used as an illustration in predicting polymer entrapment (Al-Hajri et al., 2018).*

$$I_{PV} = I_{PVo} + \Gamma_{ent} \quad (24)$$

From (24), I_{PVo} can be estimated. Considering Figure 1, the onset of polymer entrapment with reference to R_2 would commence at R_1 and the concentration value at this point is given in equation (25)

$$C_{p-ent} = C_{ag}\left[\frac{R_1}{R_h}\right]^{1/H_{R1}} \quad (25)$$

The point at which adsorption reaches its maximum and polymer entrapment becomes the dominant retention mechanism occurs at R_2 and the equivalent concentration value at this point is given in equation (26)

$$C_{p-ent} = C_{ag}\left[\frac{R_2}{R_h}\right]^{1/H_{R2}} \quad (26)$$

Similarly, pore plugging would occur at R_3 with an onset concentration shown in equation (27)

$$C_{p-plug} = C_{ag}\left[\frac{R_3}{R_h}\right]^{1/H_{R3}} \quad (27)$$

3. Materials and Method

3.1. Materials: Associative Polymer, Salts and Silica Sand

The hydrophobically associating polymer (Superpusher D118; Degree of hydrolysis: 25 – 30 mol % at 25 ^{0}C; $\overline{M_w}$: 16 – 20 x 10^6 g/mol; appearance: white granular solid; hydrophobe content: medium; total anionic content: 15 – 25 mol.%) employed in this study was manufactured and supplied by SNF Floerger, ZAC milieux, 42163 Andrezieux (France). The salts employed in the preparation of synthetic formation brine (SFB) include analytical grade sodium chloride (NaCl), magnesium chloride ($MgCl_2$), calcium chloride ($CaCl_2$), potassium chloride (KCl), sodium sulphate (Na_2SO_4), sodium hydrogen carbonate ($NaHCO_3$) and strontium chloride ($SrCl_2$). These salts were purchased from Sigma Aldrich (UK) with 99.9% purity. The commercial silica sand codenamed 40/60 was applied in the retention study. The properties of the sand and concentration of salts used are summarized in Table 3. The analysis of the grain size distribution of the silica sand was carried out using a direct sieving process using a mechanical shaker with sieve mesh arrangement (mesh size: 50 – 900 μm).

***Table 3**: Composition and properties of the commercial sand employed and synthetic brine. The synthetic brine composition was at 25 ^{0}C with pH value and specific gravity of 7.88 and 1.02 respectively.*

Synthetic Formation Brine						
Composition	**NaCl**	**KCl**	**$CaCl_2$**	**$MgCl_2$**	**Na_2SO_4**	**$NaHCO_3$**
Quantity (mg/L)	40,000	1,000	4,000	5,000	1,000	200

Commercial Silica Sand Properties				
Code Name	**Bulk Density (g/cm^3)**	**Porosity**	**Average Grain Diameter (μm)**	**Main Component**
40/60	1.724	0.364	355	Quartz (> 99.9%)

3.2. Preparation of Synthetic Brine, Stock and Dilute Polymer Solutions

Synthetic brine was formulated by dissolving varying amounts of salts in deionized water. The water was deionized to a resistivity value of 18 MΩ-cm (a threshold for removal of ions) using a Millipore™ pumping unit. The brine solutions were prepared to contain both NaCl and $CaCl_2$ in the ratios 10 to 1, respectively. Before use, the synthetic brine solution was filtered through a 0.22 μm filter paper to ensure the removal of any particles present. Stock polymer solution (5000 ppm) was prepared by dissolving polymer granules in the synthetic brine. To ensure complete dissolution, the polymer-brine mixture was stirred for 2 days using a Fischer Scientific magnetic stirrer (Model: 11-102-50SH) and allowed to hydrate for a further 24 hours. The diluted polymer solutions were prepared freshly according to the API specification RP – 63 (Recommended Practices for Evaluation of Polymers for Enhanced Oil Recovery). The concentrations of the dilute polymer solutions used for this study include the following: 10, 50, 100, 300, 500, 750, 1000 ppm.

3.3. Polymer Retention Study

3.3.1. Static Retention Test

The static retention test procedure followed the recommended practices for evaluation of polymers used in enhanced oil recovery operations (API, 1990). Commercial silica sand (100 g) was weighed into a 500 mL sample bottle. Polymer solutions (10, 50, 100, 300, 500, 750, 1000 ppm) was weighed (400 g) and added to each of the sample bottles containing the silica sand. The containers were caped and stored at representative temperatures for two days. The vessels were agitated periodically to maintain good contact between the polymer solutions and the silica sand. The polymer solutions were separated from the silica sands by filtering through a 10-micron filter. The final concentrations of the polymer solutions were estimated from viscometry using an Ubbelohde viscometer. The adsorbed polymer was calculated using equation (28) below:

$$C_{p-ad} = \frac{W_p(C_{p-i} - C_{p-f})}{M_{gr}} \quad (28)$$

Where C_{p-ad} is the amount of polymer adsorbed, W_p is the weight of polymer solution, M_{gr} is the weight of the silica sand, C_{p-i} and C_{p-f} is the initial and final polymer concentration respectively.

3.3.2. Dynamic Retention Test

The dynamic retention test procedure also followed the recommended practices for evaluation of polymers used in enhanced oil recovery operations (API, 1990). Figure 2 show a simplified diagram of the flow system used for conducting dynamic adsorption studies under different flow conditions. The pump in the flow system was set to the required injection rate (0.5 mL/min) and synthetic brine with 2.45 % Total Dissolved Solids (TDS) was injected into the porous media until the pressure stabilized. Polymer injection of the desired concentration, C_{p-inj} (**first polymer bank**) was started at the same flow rate until the pressure stabilized after

injection of about 3 pore volumes (PVs). Effluent polymer cuts from the system were collected at intervals and final effluent concentration, C_{p-eff} was estimated from viscometry using the Ubbelohde viscometer. 10 PVs (1PV = 96.4 cm^3) of brine (2.45 %TDS) was injected to flush out all non – adsorbed polymer molecules present in the sand packed core.

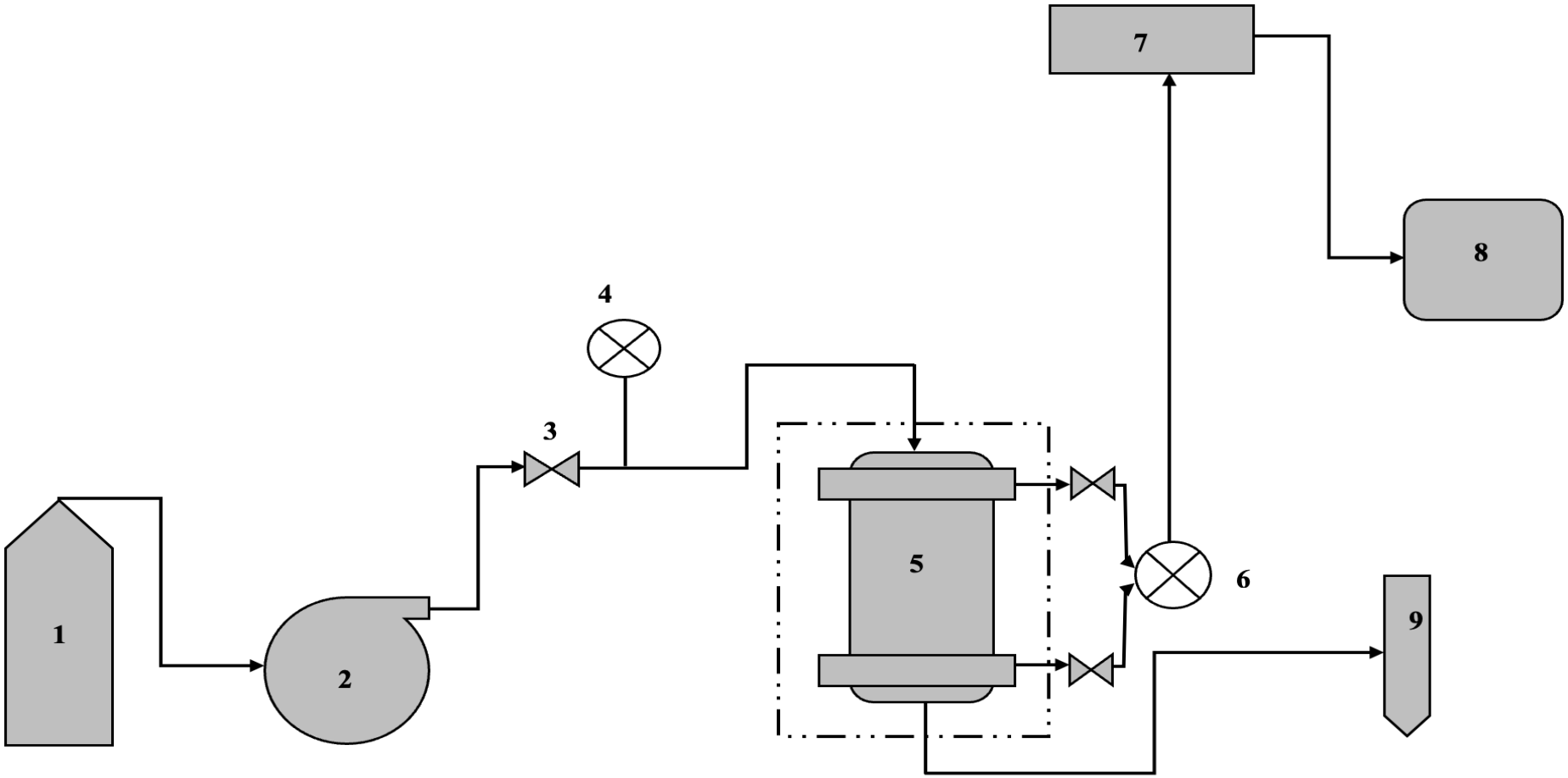

Figure 2*: Experimental setup of the core flooding apparatus. 1) pump fluid, 2) pump, 3) valves, 4) pressure gauge, 5) core holder with sand pack, 6) pressure transducer, 7) NIDAQ data logger, 8) desktop computer, 9) effluent sample collector (test tubes). The dashed line – temp control (Oven).*

The steps were repeated for the flow of a **second polymer bank** at the same concentration and flowrate through the sand-pack media. Polymer adsorption, Γ_p was estimated by comparing the plots of fractional effluent concentration curves for the first $\left(C_{p-eff}/C_{p-inj}\right)_1$ and second $\left(C_{p-eff}/C_{p-inj}\right)_2$ polymer bank against pore volume for 0.5 mL/min using equation (29) below:

$$\Gamma_p = \left(\sum\left[\left(\frac{C_{p-eff}\Delta PV}{C_{p-inj}}\right)_2 - \left(\frac{C_{p-eff}\Delta PV}{C_{p-inj}}\right)_1\right]\right)\frac{C_{p-inj}PV}{M_{gr}} \quad (29)$$

The inaccessible pore volume was computed using (30)

$$I_{PV} = 1 - PV_{\left(\frac{C_{p-eff}\Delta PV}{C_{p-inj}}\right)_2 = 0.5} \quad (30)$$

Where ΔPV is the incremental pore volume (the volume of each produced fraction of relative concentration, $\left(C_{p-eff}/C_{p-inj}\right)$) and M_{gr} is the mass of the sand pack in the core holder. The procedure was repeated for different polymer concentrations and flow rates with the retention estimated using equation (29).

3.4. Experimental Mapping of Static to Dynamic Retention

A novel experimental approach was developed for validating the predictive approach for mapping the various retention mechanisms. The correlation of static to dynamic retention was carried out using the same solid-liquid ratio and retention time. The volume of the core holder defined the volume of sand employed. Each polymer concentration was contacted with one core holder full of silica sand (with total pore volume - $PV_T = 96.4\ cm^3$). Plots of polymer retained during the static process against time were obtained for each concentration to estimate the time, $t_{max-ret}$ at which maximum retention was obtained in each case. The equivalent number of injected pore volumes, PV_{inj} during dynamic retention test for the same solid to liquid ratio and retention time obtained during the static retention test is estimated from Equation (31) below:

$$PV_{inj} = \frac{Q_{inj}t_{max-ret}}{PV_T} \quad (31)$$

Where Q_{inj} is the injected flowrate. A typical output from the correlation of the static to dynamic retention is shown in Figure 3 below. The mapping of the various retention mechanisms was done as follows:

a) **Mapping Adsorption**: adsorption is a function of the polymer contact time with the pore surface and polymer concentration.

b) **Mapping Polymer Entrapment**: entrapment is a function of the flow condition and polymer concentration in the porous media.

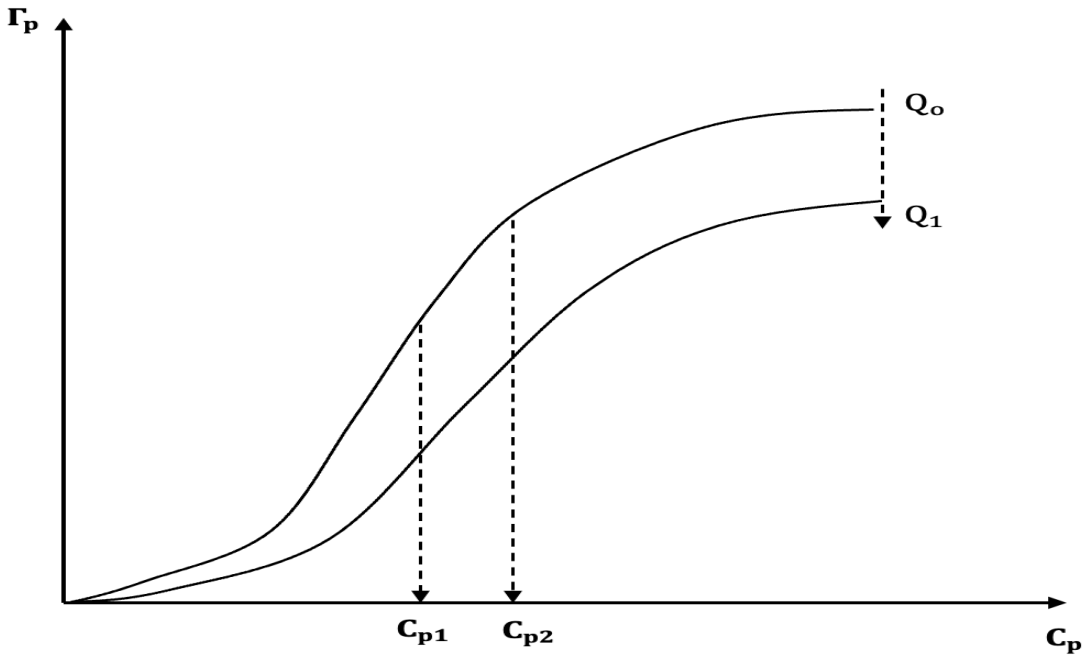

***Figure 3**: Typical out of the plot of polymer retention against concentration for the static condition at Q_o and the correlated dynamic state at flowrate Q_1.*

The rate-dependent entrapment, Γ_{ent} of polymer molecules was estimated using Equation (32), and this encompasses the area created by the vertical decrease in adsorption from Q_o to Q_1 as shown in Figure 3.

$$\Gamma_{ent} = \sum\left[\left(\frac{\Gamma_p \Delta C_p}{C_p}\right)_{Q_o} - \left(\frac{\Gamma_p \Delta C_p}{C_p}\right)_{Q_1}\right] \quad (32)$$

Where Γ_p is the estimated retention as computed using effluent concentration analysis, C_p is the polymer concentration, Q_o refers to static retention condition (zero flow condition), Q_1 is

the dynamic flow condition in the porous media, ΔC_p is the incremental polymer concentration. The concentration-dependent entrapment of polymer molecules was computed using Equation (33) and this signifies the increase in polymer concentration from C_{p_1} to C_{p_2} in Figure 3.

$$\Gamma_{ent} = \sum\left[\left(\frac{\Gamma_p \Delta C_p}{C_{p_2}}\right)_{Q_o} - \left(\frac{\Gamma_p \Delta C_p}{C_{p_2}}\right)_{Q_1}\right] - \sum\left[\left(\frac{\Gamma_p \Delta C_p}{C_{p_1}}\right)_{Q_o} - \left(\frac{\Gamma_p \Delta C_p}{C_{p_1}}\right)_{Q_1}\right] \quad (33)$$

A summary of the modified experimental procedure is given in the flow diagram in Figure 4 below.

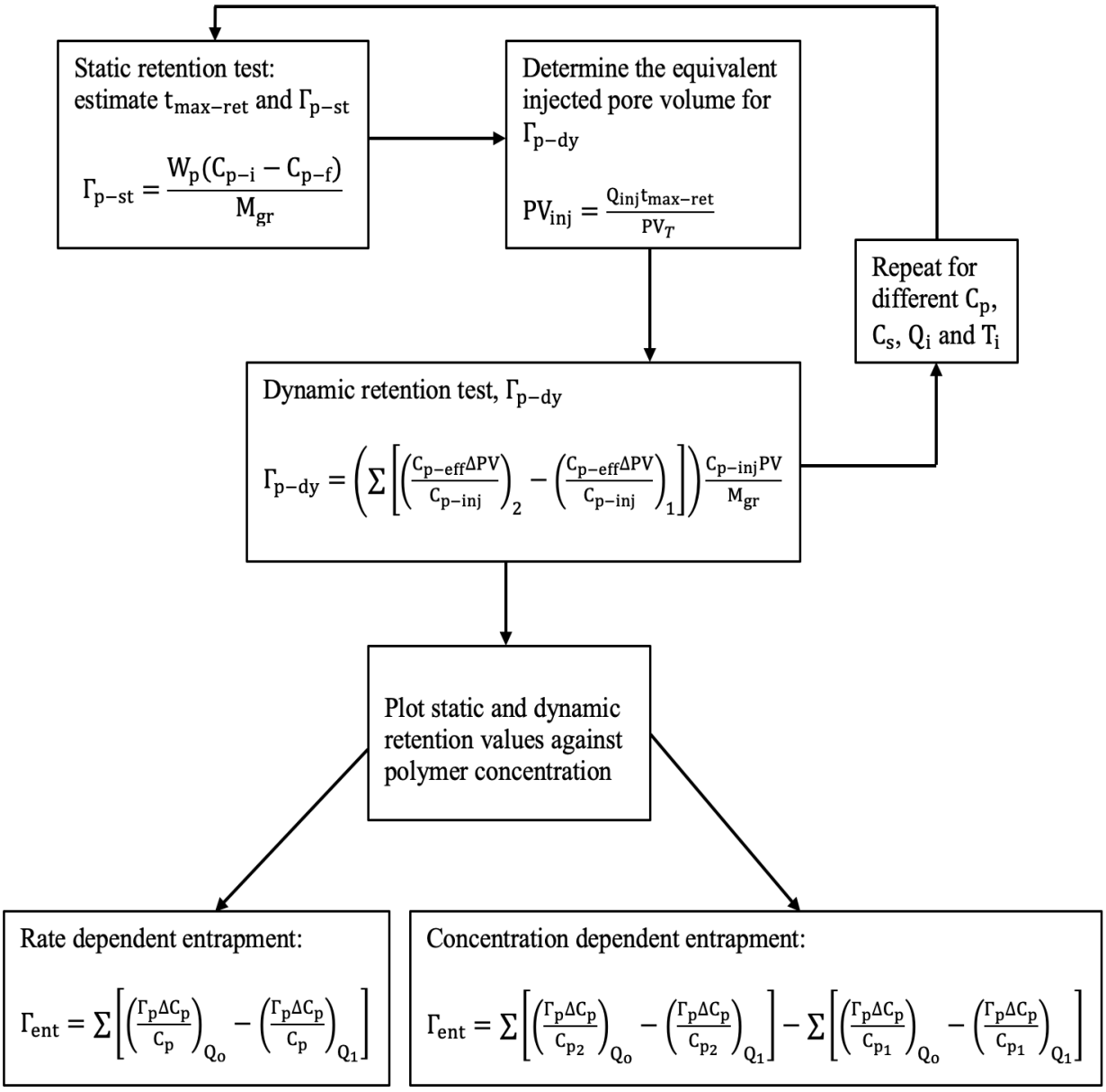

***Figure 4**: A simplified flow diagram of the modified experimental approach allows for the mapping of adsorption and entrapment mechanisms.*

4. Results and Discussion

4.1. Characterization of Silica Sand

4.1.1. Particle Size Distribution

The particle size distribution (PSD) of the silica sand (40/60) are shown in Figure 5. The PSD is important in the understanding of the sand's physical properties. The PSD will to a large extent determines the magnitude of porosity and permeability of the prepared sand packs. For the 40/60 silica sand in Figure 5, the mass mean diameter (MMD) or the D_{50} value was estimated as 350 µm.

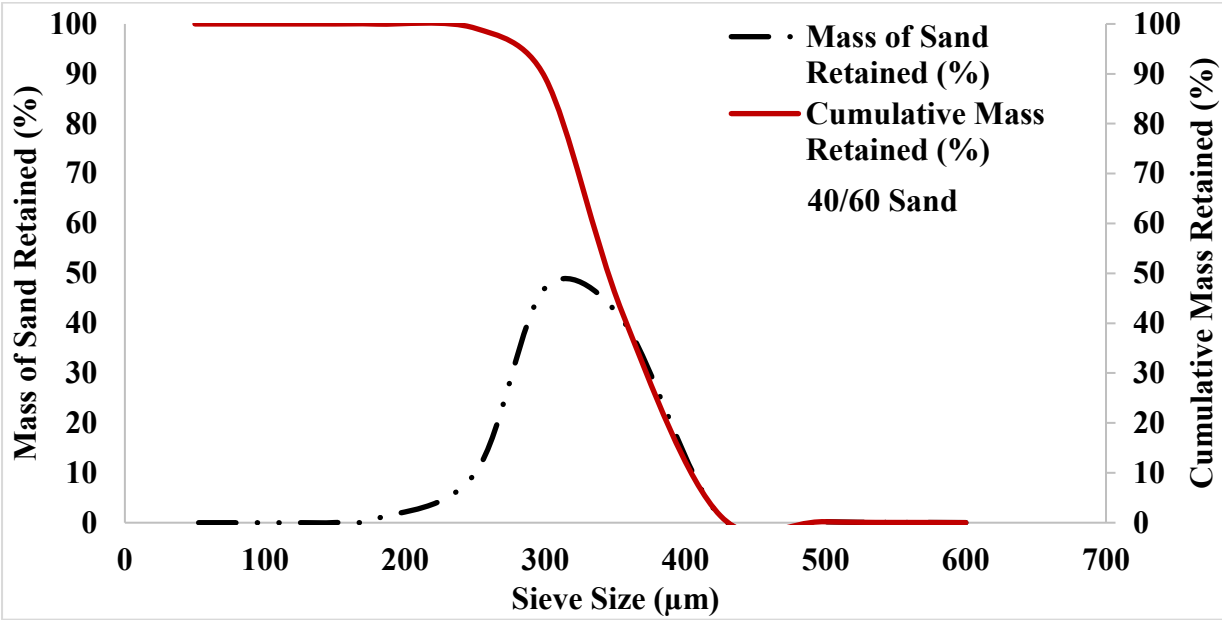

***Figure 5**: Particle size distribution of the studied sand grains (a) 40/60 sands (b) P230 sands.*

4.1.2. Transformation of Particle Size to Pore Size Distribution

The transformation of grain size to pore size distribution during packing was carried out using a modified form of the Kozeny-Carman equation for absolute permeability. The Kozeny-Carman equation is shown in equation (34)

$$k = \Phi_s^2 \frac{\phi^3 R_{gr}^2}{180(1-\phi)^2} \quad (34)$$

Where R_{gr} is the grain size of the disaggregated sand, k is the absolute permeability of the sand-packed media, Φ_s^2 is the sphericity of the particles in the packed bed, which is 1 for

spherical sand particles, ϕ is the porosity of the packed sand. The modified form of the Kozeny-Carman equation involved replacing the absolute permeability with the pore size, R_p as shown in equation (35)

$$R_p^2 = \Phi_s^2 \frac{\phi^3 R_{gr}^2}{180(1-\phi)^2} \quad (35)$$

Figure 6 shows the plot of the grain size to the corresponding transformed pore size of the sand-packed media for the silica sand. The silica sand shows an approximate normal pore size distribution with the pores more centred around a higher value.

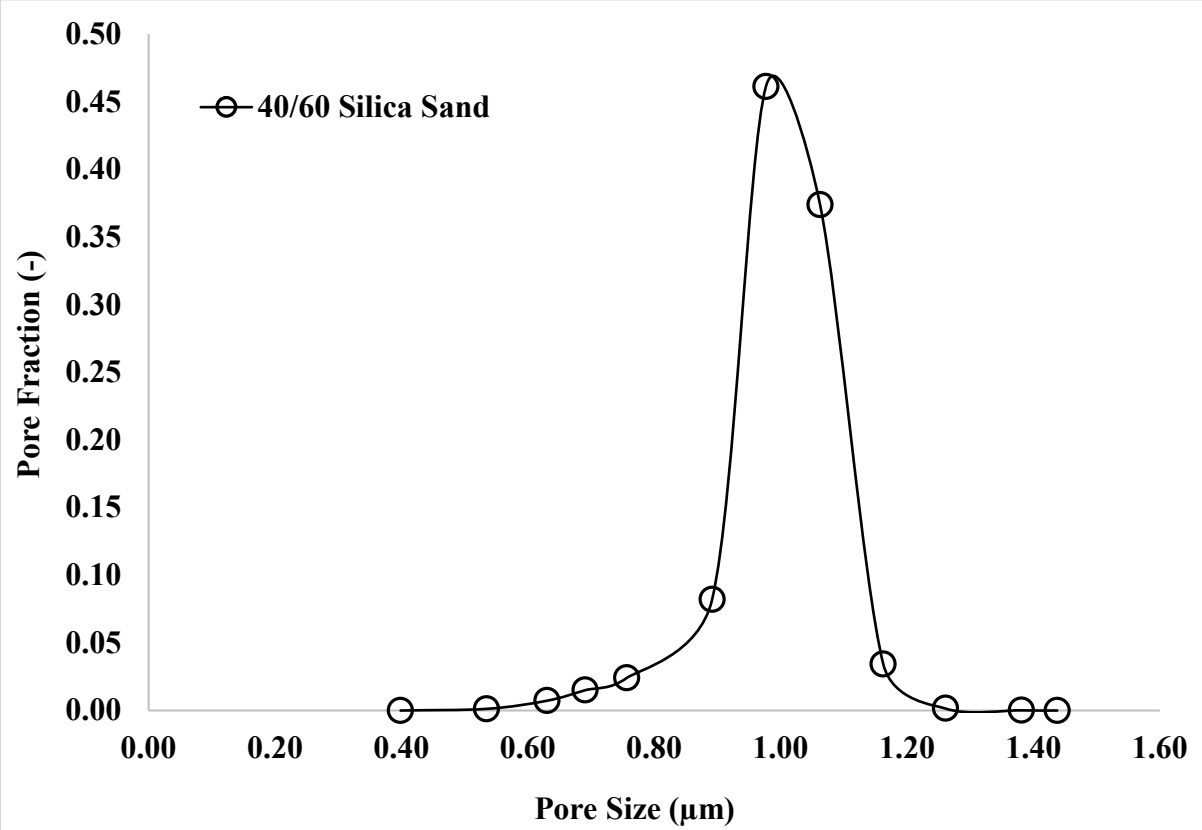

Figure 6*: Computed pore size distribution for the packed silica sand*

4.2. Predicting Polymer Retention Mechanisms: Adsorption, Entrapment and Plugging

Quantitative description of the of the various retention mechanisms puts a figure to their various contributions on the overall polymer retention in a porous media. Figure 7 shows the two plots of the cumulative pore size distribution and the cumulative size distribution of the retained polymer molecules.

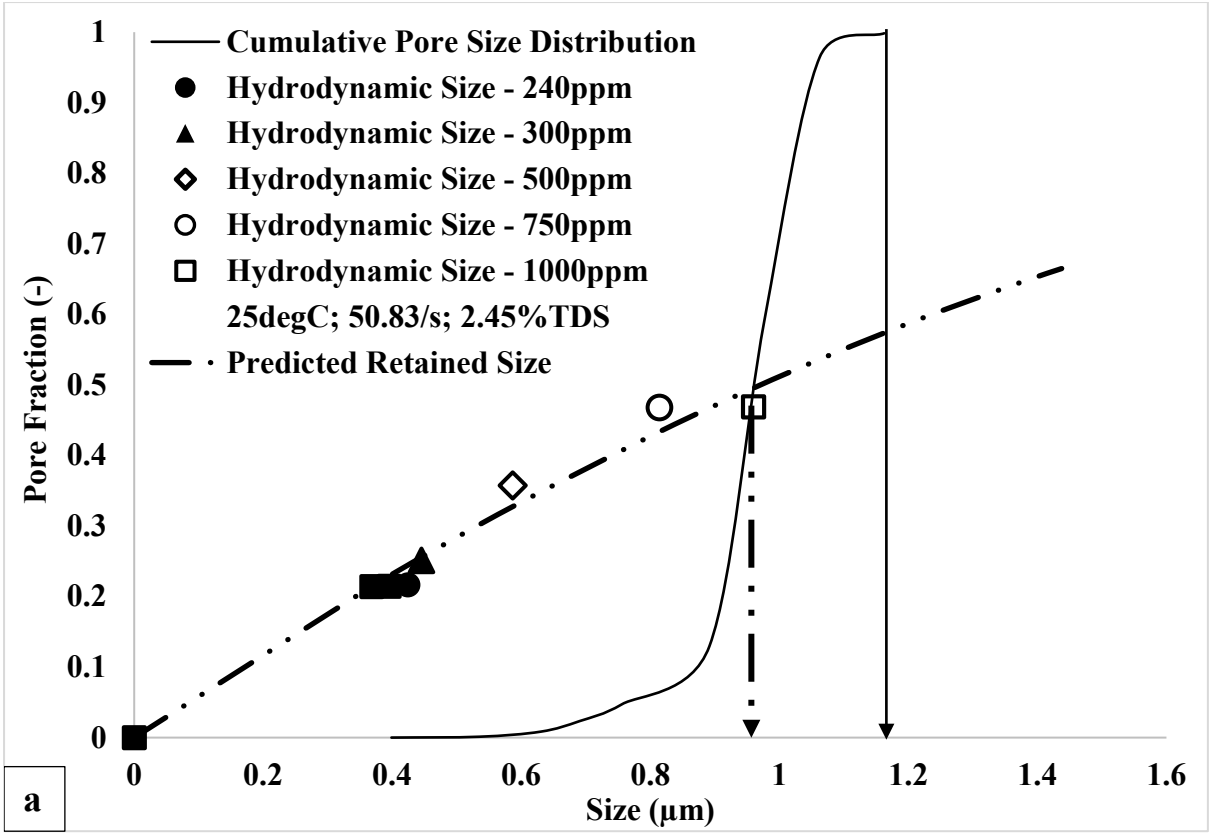

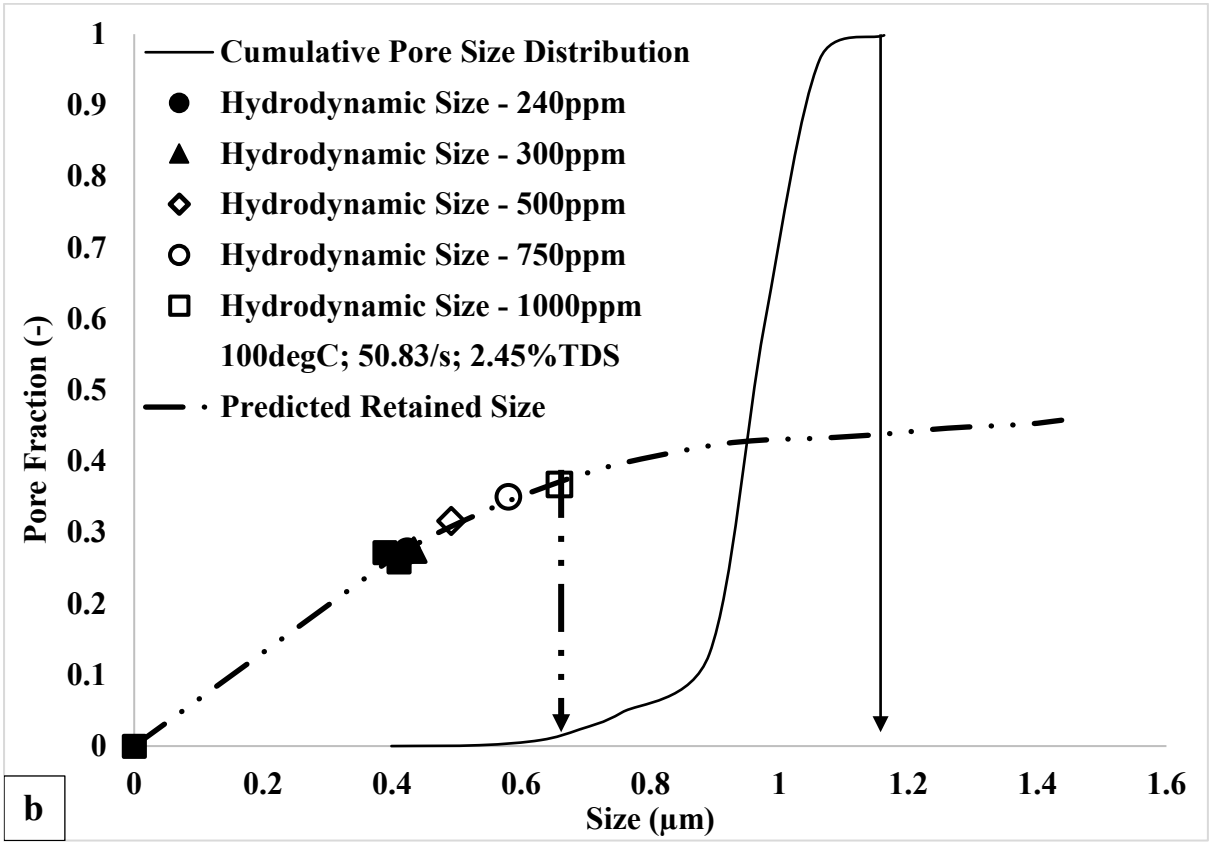

***Figure** 7: Prediction, quantification and mapping of the different retention mechanisms of associative polymers at different concentrations at 2.45 %TDS and 1 mL/min(a) 25 ℃ and (b) 100 ℃.*

For the cumulative size distribution, the area under the curve from 0.53 to 1.16 μm (as indicated by the thick arrowed line) describes the fractional pore sizes of the sand-packed media. For the second plot, the area under the curve from zero up to a size determined by the operating polymer concentration (which are represented by the different markers for the data points) described fractional size of the retained molecules. For example, the analysis of the retained polymer curve considered concentrations up to 1,000 ppm with the focus on 1,000 ppm as indicated by the dashed arrowed line in Figure 7. The hydrodynamic size of the retained polymer molecules at 1,000 ppm was estimated using equations (20) and (21). Similar estimation was done for polymer concentrations less than 1,000 ppm with Figure 8 showing the relationship between predicted size of the retained polymer molecules and the associated hydrophobic interactions against the corresponding polymer concentrations. The quantification of the different mechanisms was computed with specific focus at 1,000 ppm as indicated by the dashed arrowed line. It would be observed that for the cumulative pore size distribution at 1,000 ppm, there is an area enclosed by the dashed line. This enclosed area gives the fractional inaccessible pore (computed using equation 23) of the sand-pack which arises due to the size of the retained polymer molecules ($R_{hi} \approx R_p$). Similarly, for the cumulative size distribution of the retained molecules at 1000 ppm, it was observed that the enclosed area computed under the pore size distribution was also enclosed under this curve. However, the enclosed area under the retained size distribution would give the fraction of the entrapped molecules (computed equation 22) under the same condition ($R_{hi} \approx R_p$) rather than the fractional inaccessible pore. Table 4 show a summary of the predicted values for entrapment and inaccessible pore. However, it would also be observed from Table 4 that the predicted values for the fractional inaccessible pore, I_{PV} are greater than the predicted values for entrapment, Γ_{ent}. It was concluded from this that the difference gives the pore fraction that is completely accessible only to the brine solution, I_{PVo} and not polymer as described in equation (36)

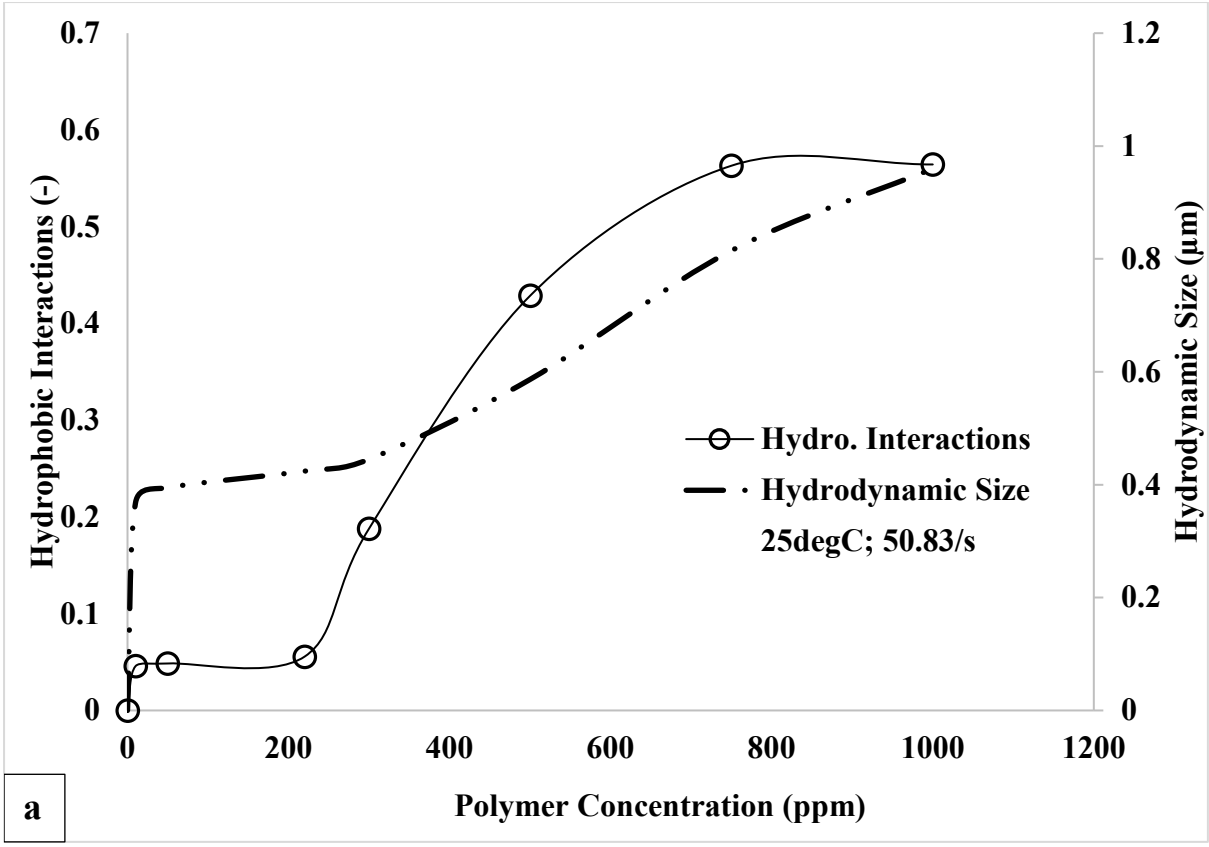

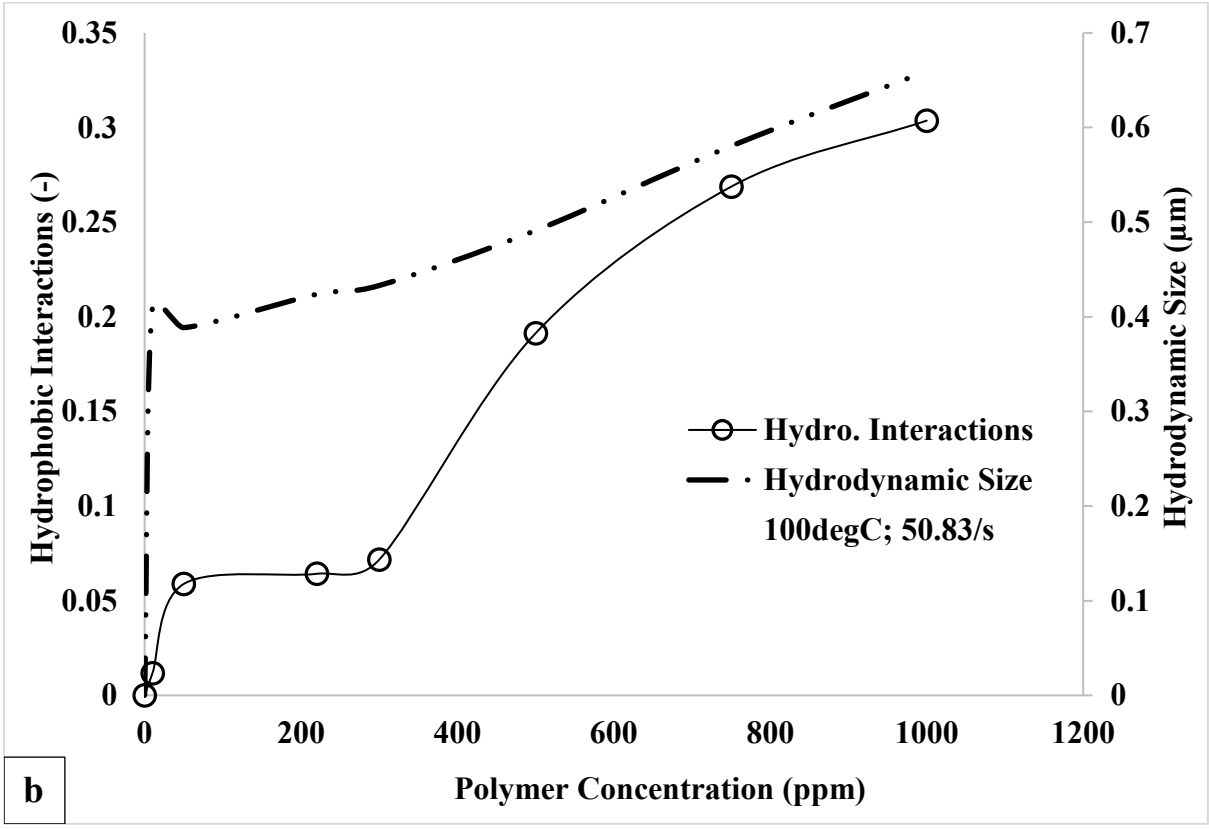

***Figure 8**: Plots of predicted hydrodynamic size of retained polymer molecules and the associated hydrophobic interactions against polymer concentrations at (a) 25 ℃ and (b) 100 ℃*

***Table 4**: Predicted values in terms of pore fraction for adsorption, entrapment and inaccessible pore volume at 25 ℃ and 100 ℃.*

25 ℃; 50.83/s			
Concentration (ppm)	**Pred. IPV.**	**Pred. Entrap.**	**Pred. Adsorp.**
300	0.006	0.001	0.999
500	0.038	0.015	0.985
750	0.155	0.085	0.915
1000	0.371	0.299	0.701

100 ℃; 50.83/s			
Concentration (ppm)	**Pred. IPV.**	**Pred. Entrap.**	**Pred. Adsorp**
300	0.0051	0.0041	0.996
500	0.0062	0.0043	0.996
750	0.0138	0.0122	0.988
1000	0.0213	0.0187	0.981

***Table 5**: Predicted concentration values for the onset of entrapment and pore plugging at 25 ℃ and 100 ℃.*

Temperature (℃)	C_{p-ent} (ppm)	C_{p-plug} (ppm)
25	437.43	1574.54
100	710.28	2669.65

$$I_{PVo} = I_{PV} - \Gamma_{ent} \quad (36)$$

Pore plugging would occur when the predicted size of retained polymer molecules exceeds the upper limit of the pore size ($R_{hi} > 1.16$ µm). Similarly, computation of the pore fractions due to adsorption was done in like manner as also contained in Table 5. The computed hydrodynamic size of the pre-injection polymer was estimated using equation (21) as 0.43 µm ($R_h = 0.43$ µm). Therefore, the predicted sizes for the retained polymer molecules less than R_h indicated retention due only to monolayer adsorption. However, beyond R_h marked the onset of multilayer adsorption coupled with entrapment of molecular aggregates ($R_h < R_{hi} < R_p$). It would be observed that the effect of temperature results in the adsorption mechanism dominating over entrapment. Increased thermal effects results in loss of polymer aggregates thereby minimizing the effect of molecular entrapment while increasing the effect of adsorption

as shown in Table 4. The onset of polymer entrapment was predicted using equation (25) and pore plugging with equation (27) as shown in Table 5. The observed trend with the predicted values for C_{p-ent} and C_{p-plug} were that they both increased with temperature with reasons due to the loss of molecular aggregates.

4.3. Experimental Validation of the Predictive Approach

Figure 9a and Figure 9b shows the polymer retention isotherm at 1 mL/min for different temperatures of 25 and 100 °C respectively. This was obtained using the developed experimental approach in Section 3.4.

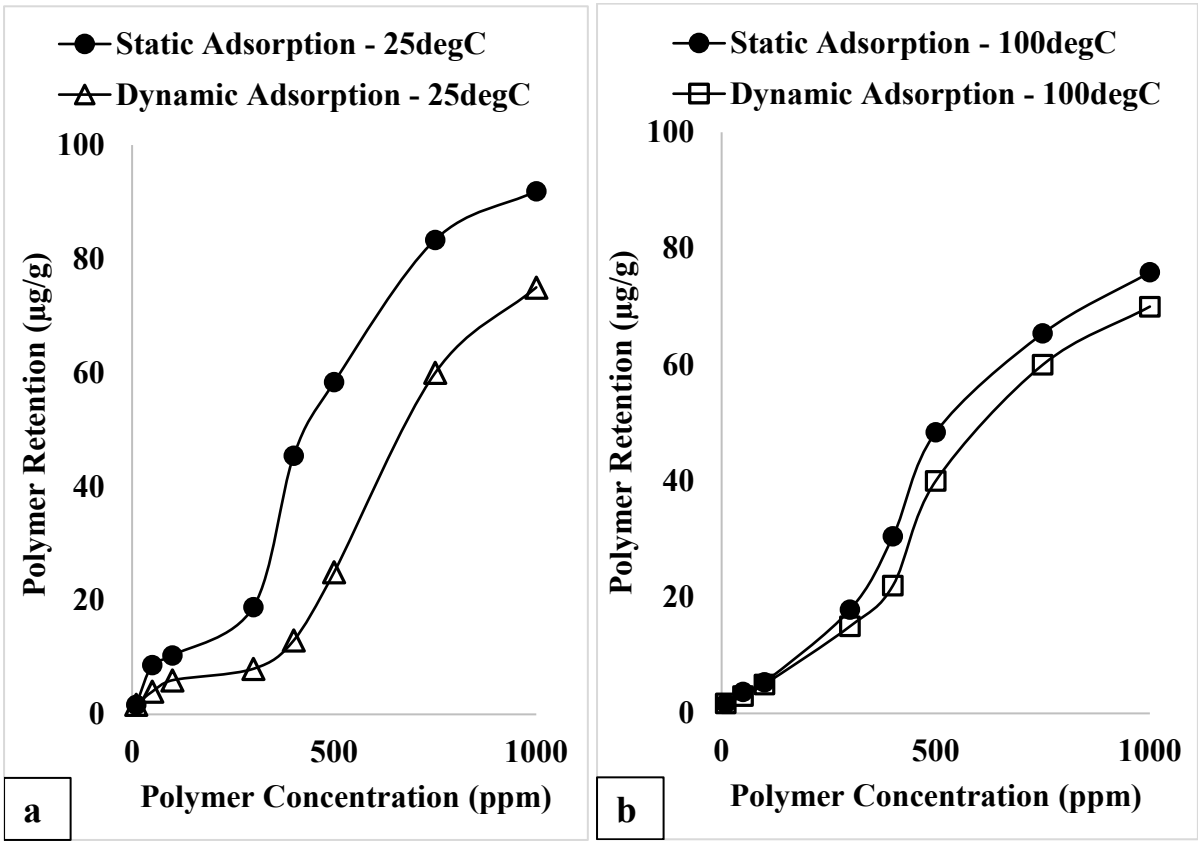

***Figure 9**: Effect of temperature on the adsorption of the associative polymer at 1 mL/min and 2.45 %TDS (a) 25°C and (b) 100°C.*

It was observed that as the temperature increased from 25 to 100 °C, the adsorption isotherm decreased. The increase in temperature results in an increase in the negative charge of the sand grains and the outcome of this is an increase in the charge repulsion between the exposed rock surface and the charged groups (carboxyl group, COO^-) on the remnant polymer molecules

attached to the rock surface. This charge repulsion ensures that remnant polymer molecules on the rock surface are detached, reducing the adsorption isotherm. Similarly, a segment of polymer molecules attached to the rock surface via hydrogen bonds or van der Waals forces is lost due to thermal degradation, resulting in a decrease in adsorption. Figure 10a and Figure 10b show the temperature effect on the entrapment of polymer molecules as estimated using Equation (2).

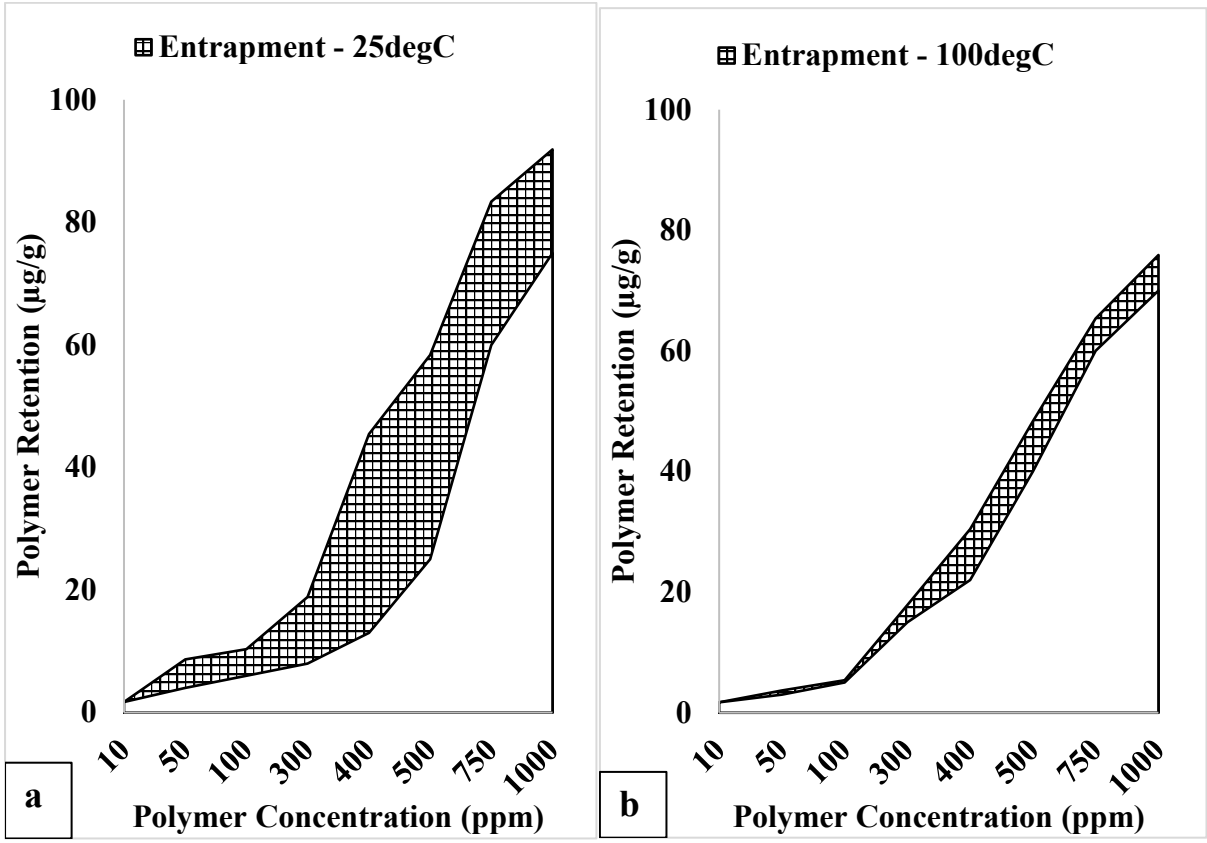

***Figure 10**: Effect of temperature on the entrapment of polymer molecules on the 40/60 silica sand saturated with 2.45 %TDS brine solution and at 1 ml/min.*

Polymer molecular aggregates are responsible for the entrapment mechanism in the porous media, and this arises when the size of the aggregate is about the size of the pore throat. However, the increased temperature conditions allowed for the degradation of intermolecular interaction responsible for this, thereby reducing the size of the aggregates. This would allow for easy transport of the polymer molecules through the pore throat with reduced retention; however, the loss of the intermolecular interaction would significantly affect the mobility

control mechanism of the polymer solution. Tables 6 and 7 shows a summary of the predicted and the experimental outcomes for the various retention mechanisms related to the associative polymer.

***Table 6**: Predicted and experimental values of adsorption in terms of pore fraction at 25 ℃ and 100 ℃.*

25℃; 50.83/s (1 mL/min)		
Concentration (ppm)	**Pred. Adsorption.**	**Exp. Adsorption.**
300	0.999	0.899
500	0.985	0.885
750	0.915	0.795
1000	0.701	0.852

100℃; 50.83/s (1 mL/min)		
Concentration (ppm)	**Pred. Adsorption**	**Exp. Adsorption.**
300	0.996	0.892
500	0.996	0.953
750	0.988	0.923
1000	0.981	0.933

In order to compare the effectiveness of the predictive approach in estimating the outcomes of the experimental approach, the coefficient of determination, R^2 was applied in the correlation of the predicted outcome to the experimental outcome. For adsorption, the coefficient of determination, R^2 was 90.45% at 25℃, while at 100℃, the R^2 was 88.05%. The RMSE values at 25℃ was 0.0597 while at 100℃ the value was 0.0346. In the case of entrapment, the coefficient of determination, R^2 was 87.43% at 25℃, while at 100 ℃, the R^2 is 87.05%. The RMSE values at 25℃ was 0.0413 while at 100℃ the value was 0.00367. The seemingly significant correlation between the predicted outcome and the experimental outcome shows that the developed experimental approach can be used for the quantitative mapping of the

polymer adsorption distinctively from the other types of polymer retention mechanisms attributable to associative polymers.

***Table** 7: Predicted and experimental values of polymer entrapment in terms of pore fraction at 25 ℃ and 100 ℃.*

25℃; 50.83/s (1mL/min)		
Concentration (ppm)	**Pred. Entrapment.**	**Exp. Entrapment.**
300	0.001	0.09
500	0.015	0.10
750	0.085	0.15
1000	0.299	0.21

100℃; 50.83/s (1mL/min)		
Concentration (ppm)	**Pred. Entrapment.**	**Exp. Entrapment.**
300	0.0041	0.001
500	0.0043	0.012
750	0.0122	0.020
1000	0.0187	0.028

5. Conclusion and Recommendations

The various types of retention mechanisms linked with associative polymers during transport in porous media were quantitatively described in this work. The uniqueness of the predictive approach is that it allowed for the determination of the critical concentration which would mark the onset of the loss of molecular aggregates responsible for polymer viscous property to entrapment and plugging. All this was achieved with the knowledge of the contributory effect of the associated hydrophobic interactions which exists between the retained polymer molecules. Consequently, proper economic planning and computational forecasting of the performance of associative polymers can be made with the predictive approach. However, the predictive approach for mapping the different retention types was developed using disaggregated sand. This makes the estimation of the cumulative size distribution of the

retained polymer molecules strictly via a predictive approach. Nonetheless, a novel experimental approach was developed to validate the predictive approach by corelating static to dynamic retention. The outcome of the validation showed a significant corelation between the predictive and experimental outcome. However, an accurate representation of the experimental outcome could be achieved using a consolidated porous media. The difference between the pre-distribution and post-distribution curves for the consolidated media would give the size distribution of retained polymer molecules in the consolidated porous media and this is an area of further works being carried out.

Acknowledgement

The authors would like to acknowledge the financial grant (PTDF/ED/PHD/ARO/1387/18) from the Petroleum Technology Development Fund (PTDF) Nigeria for this research work. Also, the authors acknowledge the comments and contributions of the various anonymous reviewers of this article.

Conflict of Interest

The authors declare that there is no conflict of interest regarding the publication of this article.

References

Afolabi, R. O. (2015). Effect of Surfactant and Hydrophobe Content on the Rheology of Poly(acrylamide-co-N-dodecylacrylamide) for Potential Enhanced Oil Recovery Application. *American Journal of Polymer Science, 5*(2), 41-46.

Afolabi, R. O., Oluyemi, G. F., Officer, S., & Ugwu, J. O. (2019). Hydrophobically Associating Polymers for Enhanced Oil Recovery – Part B: A Review of Modelling Approach to Flow in Porous Media. *Journal of Molecular Liquids, 293*, 1-14.

Afolabi, R. O., Oluyemi, G. O., Officer, S., & Ugwu, J. O. (2019). Hydrophobically Associating Polymers for Enhanced Oil Recovery – Part A: A Review on the Effects of Some Key Reservoir Conditions. *Journal of Petroleum Science and Engineering, 180*, 681-698.

Afolabi, R. O., Oluyemi, G. F., Officer, S., & Ugwu, J. O. (2020). Determination of a Critical Separation Concentration for Associative Polymers in Porous Media based on Quantification of Dilute and Semi-Dilute Concentration Regimes. *Journal of Molecular Liquids, 317*, 114142.

Al-Hajri, S., Mahmood, S. M., Abdulehah, H., & Akbari, S. (2018). An Overview on Polymer Retention on Porous Media. *Energies, 11*(10), 2751.

Al-Hajri, S., Mahmood, S. M., Abdulrahman, A., Abdulelah, H., Akbari, S., & Saraih, N. (2019). An Experimental Study on Hydrodynamic Retention of Low and High Molecular Weight Sulfonated Polyacrylamide Polymer. *Polymers, 11*(9), 1453.

Al-Hajri, S., Mahmood, S. M., Akbari, S., Abdulelah, H., Yekeen, N., & Saraih, N. (2020). Experimental Investigation and Development of Correlation for Static and Dynamic Adsorption in Porous Media. *Journal of Petroleum Science and Engineering, 189*, 106864.

Bai, Y., Shang, X., Wang, Z., & Zhao, X. (2018). Experimental Study on Hydrophobically Associating Hydroxyethyl Cellulose Flooding System for Enhanced Oil Recovery. *Energy and Fuels, 32*, 6713-6725.

Bernabé, Y., Zamora, M. Li, A. Maineult, M. & Tang, Y. B. (2011). Pore Connectivity, Permeability, and Electrical Formation Factor: A New Model and Comparison to Experimental Data, *Journal of Geophysical Research*, **116**, B11204, doi:10.1029/2011JB008543.

El-Hoshoudy, A. N., Desouky, S. E., Al-Sabagh, A. M., Betiha, M. A., El-Kady, M. Y., & Mahmoud, S. (2017). Evaluation of Solution and Rheological Properties for Hydrophobically Associated Polyacrylamide Copolymer as a Promised Enhanced Oil Recovery Candidate. *Egyptian Journal of Petroleum, 26*, 779-785.

Guo, Y. J., Hu, J., & Zhang, X. M. (2016). Flow Behavior through Porous Media and Microdisplacement Performance of Hydrophobically Modified Partially Hydrolyzed Plyacrylamide. *SPE Journal, 21*(3), 688-705.

Guo, Y. J., Liu, J.-x., Zhang, X., Feng, R., Li, H., Zhang, J., . . . Luo, P. (2012). Solution Property Investigation of Combination Flooding Systems Consisting of Gemini–Non-ionic Mixed Surfactant and Hydrophobically Associating Polyacrylamide for Enhanced Oil Recovery. *Energy and Fuels, 26*(4), 2116–2123.

Idahosa, P. E. G., Oluyemi, G. F., Oyeneyin, M. B. & Prabhu, R. (2016). Rate-Dependent Polymer Adsorption in Porous Media. *Journal of Petroleum Science and Engineerin*g. *143*, 65-71

Jincheng, M., Tan, H., Yang, B., Zhang, W., Yang, X., Zhang, Y., & Zhang, H. (2018). Novel Hydrophobic Associating Polymer with Good Salt Tolerance. *Polymers, 10*(8), 1-19.

Kajjumba, G. W., Emik, S., Ongen, A., Ozkan, H. K., & Aydin, S. (2018). Modelling of Adsorption Kinetic Processes - Errors, Theory and Application, Advanced Sorption Process Applications, Serpil Edebali, IntechOpen, DOI: 10.5772/intechopen.80495. Available from: https://www.intechopen.com/chapters/63161

Kamal, M. S., Sultan, A. S., Al-Mubaiyedh, U. A., & Hussein, I. A. (2015). Review on Polymer Flooding: Rheology, Adsorption, Stability, and Field Applications of Various Polymer Systems. *Polymer Reviews*, 1-40.

Li, Q., Pu, W., Wei, B., Jin, F., & Li, K. (2016). Static Adsorption and Dynamic Retention of an Anti-Salinity Polymer in Low Permeability Sandstone Core. *Journal of Applied Polymer Science, 134*(8), 44487-44494.

Li-Bin, D., Dong-Qing, Z., Shou-Ping, L., & Yun-Xiang, Z. (2010). Effects of Ethylene Oxide Spacer Length on Solution Properties of Water-Soluble Fluorocarbon-Containing Hydrophobically Associating Poly (Acrylic Acid-co-Rf-PEG Macromonomer). *Chinese Journal of Chemistry, 21*(6), 698-705.

Lohne, A., Nodland, O., Stavland, A., & Hiorth, A. (2017). A Model for Non-Newtonian Flow in Porous Media at Different Flow Regimes. *Computational Geosciences, 21*, 1289-1312.

Quan, H., Li, Z., & Huang, Z. (2016). Self-Assembly Properties of a Temperature and Salt Tolerant Amphoteric Hydrophobically Associating Polyacrylamide. *RSC Advances, 6*, 49281-49288.

Quan, H., Lu, Q., Chen, Z., Huang, Z., & Jiang, Q. (2019). Adsorption-Desorption Behavior of the Hydrophobically Associating Copolymer AM/APEG/C-18/SSS. *RSC Advances, 9*, 12300-12309.

Revil, A., Koch, K. & Holliger, K. (2012). Is it the Grain Size or the Characteristic Pore Size that Controls the Induced Polarization Relaxation Time of Clean Sands and Sandstones? *Water Resources Research*, 48(5), 1 - 7.

Seright, R. S., Fan, T., Wavrik, K., Wan, H., Galliard, N., & Favero, C. (2011). Rheology of a New Sulfonic Associative Polymer in Porous Media. *SPE Reservior Evaluation and Evaluation, 14*(6), 726-734.

Torrealba, V. A., & Hoteit, H. (2019). Improved Polymer Flooding Injectivity and Displacement by Considering Compositionally-Tuned Slugs. *Journal of Petroleum Science and Engineering, 178*, 14-26.

Yekeen, N., Manan, M. A., Idris, A. K., & Samin, A. M. (2017). Influence of Surfactant and Electrolyte Concentrations on Surfactant Adsorption and Foaming Characteristics. *Journal of Petroleum Science and Engineering, 149*, 612-622.

Zhang, G. (2013). New Insights into Polymer Retention in Porous Media. Thesis, New Mexico Institute of Mining and Technology.

Zhang, G., & Seright, R. (2014). Effect of Concentration on HPAM Retention in Porous Media. *SPE Journal, 19*(3), 373-380.